JOURNAL OF PROPULSION AND POWER
Vol. 26, No. 5, September–October 2010

Calculating an Admittance Function from Pulsed Tubular Grain Motor Tests

C. W. Rousseau* and J. H. Knoetze†
University of Stellenbosch, Matieland 7602, South Africa

DOI: 10.2514/1.40286

Obtaining the admittance function for propellants is an important part of combustion instability analysis. However, obtaining an admittance function is an expensive process. The T-burner is the industry standard method for characterizing acoustic response of solid propellants. This device is expensive to maintain and operate due to large test matrices required to quantify the response for a single propellant. To reduce costs, a method was developed for obtaining admittance functions from a pulsed tubular grain. This method allows for several modes to be evaluated simultaneously and in so doing reduces the total number of tests. A reusable tubular grain motor that can be pulse-tested was designed. Two methods were used to evaluate the data, namely Culick's nonlinear gas dynamics method and Flandro's energy balance method. These methods returned similar results. Linear analysis (as developed by Flandro and coworkers) was performed. A baseline propellant was first evaluated, three motors with 1% SiC as a stability additive, and two motors with 4% Al. Good agreement was found between the two methods. The SiC, which is not a common additive, was found to greatly increase the stability of the motor. One tubular pulsed test has the potential to replace at least 15 T-burner tests.

Nomenclature

A_b	=	admittance function for the burning surface
A_n,B_n	=	defined by Eq. (15)
Ar_n	=	defined by Eq. (2)
a	=	speed of sound, m s^{-1}
C_m	=	weight ratio particles to gas
C_v	=	specific heat at constant volume, J mol^{-1} K^{-1}
E	=	time-averaged energy density
E_m^2	=	energy normalization function
k_m	=	wave number for axial mode m, $n\pi R/L$
L	=	length of the motor, m
M_b	=	Mach number at the burning surface
n_b	=	linear burn rate law exponent
n	=	mode number
P	=	chamber pressure, MPa
Pr	=	the Prandtl number
p'	=	acoustic pressure, MPa
r	=	radial position, m
r_n	=	amplitude of the nth mode
S	=	surface area, m^2
s	=	entropy, J kg^{-1} K^{-1}
U	=	mean flow velocity, m s^{-1}
U_r, U_z	=	mean flow velocity components, m s^{-1}
u	=	gas velocity, m s^{-1}
$\mathbf{u}$	=	oscillatory velocity vector
V	=	volume, m^3
v	=	velocity, m s^{-1}
z	=	axial position, m
α	=	growth or decay constants, s^{-1}
β_c	=	nonlinear gas dynamics term arising from Culick's method
β_{DC}	=	mean pressure constant from Eq. (6)
γ	=	ratio of specific heats
δ_d^2	=	viscous dialational function $\delta_d^2 \equiv \delta_{Re}^2(2 + \lambda/\mu)$
δ_{Re}^2	=	inverse square root of the acoustic Reynolds number based on the radius
$\epsilon(t)$	=	instantaneous pressure amplitude ratio, p'/P_0
η_n	=	defined by Eq. (15)
λ	=	second coefficient of viscosity
μ	=	dynamic viscosity of the gas, kg m^{-1} s^{-1}
ρ	=	density, kg m^{-3}
τ_d	=	particle relaxation time, s
θ_n	=	frequency shifting of the nth mode
ψ_n	=	mode shape of the nth mode
ω_n	=	angular frequency of the nth mode

Subscripts

0	=	indicates the quiescent chamber reference conditions
*	=	dimensional quantity
lim	=	indicates the limiting amplitude is reached
(r), (i)	=	refers to the real and imaginary parts
b	=	burning propellant surface
std	=	predicted value

Superscripts

(1)	=	denotes first-order accuracy
$\hat{(\,)}$	=	acoustic (irrotational) part
$\overline{(\,)}$	=	indicated the mean value
$\tilde{(\,)}$	=	vortical (rotational) part

Presented as Paper 2008-4599 at the 44th AIAA/ASME/SAE/ASEE Joint Propulsion Conference & Exhibit, Hartford CT, 21–23 July 2008; received 6 August 2008; revision received 27 November 2009; accepted for publication 11 January 2010. Copyright © 2010 by University of Stellenbosch. Published by the American Institute of Aeronautics and Astronautics, Inc., with permission. Copies of this paper may be made for personal or internal use, on condition that the copier pay the $10.00 per-copy fee to the Copyright Clearance Center, Inc., 222 Rosewood Drive, Danvers, MA 01923; include the code 0748-4658/10 and $10.00 in correspondence with the CCC.

*Ph.D. Student, Department of Process Engineering, Private Bag X1.
†Professor, Department of Process Engineering, Private Bag X1; jhk@sun.ac.za.

I. Introduction

COMBUSTION instability is a common problem experienced in solid rocket motors. The ability to accurately predict the combustion stability of a motor is strongly influenced by the quality of the available experimental data for a propellant. T-burners are the industry standard but requires a large test matrix. This makes it expensive to operate and maintain.

This study will show that the total number of tests required to be able to adequately predict a solid rocket motor's combustion stability can be reduced. The basic concept of the T-burner is expanded to a tubular grain motor. The ever improving linear stability analysis is applied to calculate loss and gain mechanisms, which previously would be measured experimentally during a T-burner test to find the

response of the propellant. A new analysis of the burn time data is developed that allows multiple modes to be evaluated simultaneously. This allows for a broad frequency range to be investigated. This analysis also allows triggering to be evaluated which is not possible with a T-burner.

A cylindrical grain motor is pulsed 3 times during the burn time. If the motor does not go unstable it is possible to determine the growth or decay constants, α for multiple longitudinal modes at three different pressures. When the motor is linearly stable the classical linear analysis and Flandro's energy balance analysis is used. Both Culick's and Flandro's nonlinear method were applied when the motor is unstable after pulsing.

The α values of different modes can then be used to obtain the admittance function for the propellant. Improved linear stability integrals are used to account for all other gain and loss mechanisms. This will be limited to the first five modes due to constraints resulting from assumptions made to solve the linear stability integrals.

The data from three motors were evaluated. A base line propellant with no stability additives, a motor with 1% SiC, and a motor with 4% Aluminum. SiC is not commonly used as a stability additive and will be evaluated as a viable alternative to ZrC.

II. Test Motor

The test motor was designed to be pulsed 3 times and also to be reusable [1]. The bulk head was modified to accommodate three pulsers, two dynamic transducers and one static pressure transducer. To allow for reuse, the grain (10 kg propellant) can be cast into a reusable sleeve. This allows for the motor grain to be easily inserted and removed. The nozzle can easily be interchanged to allow for different pressures to be evaluated. The motor is 1.4 m in length allowing for a frequency range of 350–2000 Hz to be evaluated. The frequency range can be altered by changing the length of the motor. The pulsers were all identical with rupture pressures between 30–35 MPa depending on motor pressure. It was desired that the maximum rupture pressure be achieved as to give best chance of causing instability.

III. Mathematical Strategy

Analysis of the stability of solid rocket motors can be divided into two distinct areas, namely linear and nonlinear stability analysis. Flandro and coworkers [2–9] have published extensively on improving the linear stability prediction. It has been shown that these new stability integrals have improved theoretical prediction capabilities, as shown by Flandro [7]. Linear theory has been well established for longitudinal waves in cylindrical motors.

Nonlinear stability has been a subject of much debate (cf. Culick [10]). Two methods will be used in this study, namely Culick's nonlinear gas dynamics method and Flandro's energy balance method. French [6] has shown that Culick's and Flandro's methods give the same results as prediction tools for cylindrical motors. Here they will be applied as analysis tools.

A. Composite Wave Assumption and Superposition

Culick [10–12], Flandro et al. [7–9], and Flandro [13,14] have shown that analysis is greatly simplified by realizing that the waves are composites of the chamber normal modes. The composite steep fronted wave can be described [7–9,13,14] with:

$$p'(\mathbf{r},t) = \epsilon(t)\sum_{n=1}^{\infty} Ar_n(t)\psi_n(\mathbf{r}) \tag{1}$$

For a port with constant cross section

$$\begin{cases} Ar_n(t) = \left(\frac{8n}{4n^2+1}\right)\sin\left(\frac{n\pi a_0}{L}\right) \\ \psi_n(r) = \cos\left(\frac{n\pi z}{L}\right) \end{cases} \tag{2}$$

This approach has been shown to conform to all experimental features and greatly reduces computational effort. Thus, it is also possible to use a fast Fourier transform (FFT) algorithm to decompose the wave in to the individual modes.

B. Linear Stability Integrals

There has been extensive work done on improving the linear stability integrals (Chibli et al. [2], Flandro and Majdalani [3], Fischbach et al. [4,5], French [6], and Flandro et al. [7–9]). The main focus is to incorporate the vorticity. The derivation of these can be found in the original papers and will not be given here. The integrals are listed in Table 1. The total motor growth constant α_m is given as

$$\alpha_m = \alpha_1 + \alpha_2 + \alpha_3 + \cdots = \sum_{i=1}^{N}\alpha_i \tag{3}$$

α_1 is the pressure-coupled response and the nozzle losses, α_2 is the dilation energy correction, α_3 the acoustic mean flow correction. α_4, the flow turning correction and α_5, the rotational flow correction have been shown to be equal and opposite in sign [2,3] as have α_9 the pseudorotational correction and α_{10} the unsteady nozzle correction [2,15]. α_6 is the mean vortical correction, α_7 is the viscous correction, and α_8 the pseudo acoustical correction that can generally be ignored as it is of the order M_b^3. The mode stability will be determined as follows:

Table 1 Stability integrals and results for tubular grain motor

αs	Volume integral [3]	Surface integral [4]	Tubular grain [3]
α_1	$\frac{E_m^{-2}}{\exp(2\alpha_m t)}\iiint_V \left\langle \begin{matrix} -\nabla\cdot[(\hat{p}\cdot\hat{\mathbf{u}})+\frac{1}{2}M_b(U\cdot\hat{p}^2)] \\ -M_b[\hat{\mathbf{u}}\cdot\nabla(\mathbf{U}\times\hat{\mathbf{u}})] \end{matrix}\right\rangle \mathrm{d}V$	$\frac{E_m^{-2}}{\exp(2\alpha_m t)}\iint_S \left\langle \begin{matrix} \mathbf{n}\cdot[(\hat{p}\cdot\hat{\mathbf{u}})+\frac{1}{2}M_b(U\cdot\hat{p}^2)] \\ -M_b[\hat{\mathbf{u}}\cdot\mathbf{n}(\mathbf{U}\times\hat{\mathbf{u}})] \end{matrix}\right\rangle \mathrm{d}S$	$\frac{\pi M_b}{2E_m^2}\frac{L}{R}\left\{\begin{matrix}[A_b^{(r)}+1] \\ -[\gamma+1]\end{matrix}\right\}$
α_2	$\frac{E_m^{-2}}{\exp(2\alpha_m t)}\iiint_V \langle\delta_d^2\hat{\mathbf{u}}\cdot\nabla(\nabla\cdot\hat{\mathbf{u}})\rangle\,\mathrm{d}V$	$\frac{4k_m\delta_{Re}^2}{3\exp(2\alpha_m t)E_m^2}\iint_S\langle n\cdot(\hat{p}\,\hat{\mathbf{u}})\rangle\,\mathrm{d}S - \frac{2}{3}\delta_{Re}^2k_m^4$	$\simeq -\frac{\delta_d^2\pi k_m^2}{4E_m^2}\frac{L}{R}$
α_3	$\frac{E_m^{-2}}{\exp(2\alpha_m t)}\iiint_V \langle M_b[\hat{\mathbf{u}}\cdot(\hat{\mathbf{u}}\times\Omega)]\rangle\,\mathrm{d}V = \mathcal{O}(M_b^2)$	Negligible	Negligible
α_4	$\frac{E_m^{-2}}{\exp(2\alpha_m t)}\iiint_V \langle M_b\hat{\mathbf{u}}\cdot(\mathbf{U}\times\omega_v)\rangle\,\mathrm{d}V$	$\frac{M_bE_m^{-2}}{\exp(\alpha_m t)}\langle\tilde{\mathbf{u}}^{(i)}\cdot\hat{\mathbf{u}}\rangle\,\mathrm{d}S S_b$	$\simeq -\frac{\pi M_b}{2E_m^2}\frac{L}{R}$
α_5	$\frac{E_m^{-2}}{\exp(2\alpha_m t)}\iiint_V \langle-\tilde{\mathbf{u}}\cdot\nabla\hat{p}\rangle\,\mathrm{d}V$	$\frac{E_m^{-2}}{\exp(2\alpha_m t)}\iint_S\langle\mathbf{n}\cdot(\tilde{\mathbf{u}}\,\hat{p})\rangle\,\mathrm{d}S$	$\simeq \frac{1}{2}(\frac{\pi M_b}{E_m^2})\frac{L}{R}$
α_6	$\frac{E_m^{-2}}{\exp(2\alpha_m t)}\iiint_V \langle M_b\tilde{\mathbf{u}}\cdot(\mathbf{U}\times\omega_v)\rangle\,\mathrm{d}V$	$\frac{M_bE_m^{-2}}{\exp(2\alpha_m t)}\iint_S\langle\mathbf{n}\cdot\mathbf{U}(\frac{1}{2}\tilde{\mathbf{u}}\cdot\tilde{\mathbf{u}})\rangle\,\mathrm{d}S$	$\simeq \frac{\pi M_b L}{4E_m^2R}$
α_7	$\frac{E_m^{-2}}{\exp(2\alpha_m t)}\iiint_V \langle-\delta_{Re}^2(\hat{\mathbf{u}}\cdot\tilde{\mathbf{u}})\cdot(\nabla\times\omega_v)\rangle\,\mathrm{d}V$	$\frac{-\delta_{Re}^2k_m^2}{2E_m^2\exp(2\alpha_m t)M_b^2}\iint_S\langle\tilde{\mathbf{u}}^2\rangle\vert_{r=1}\,\mathrm{d}S$	$\simeq -\frac{\pi\delta_{Re}^2}{6E_m^2}\frac{L}{R}(\frac{k_m}{M_b})^2 = -\frac{\pi M_b\xi}{6E_m^2}\frac{L}{R}$
α_8	$-\frac{E_m^{-2}}{\exp(2\alpha_m t)}\iiint_V\langle-\hat{\mathbf{u}}\cdot\nabla\tilde{p}\rangle\,\mathrm{d}V \simeq \frac{M_b^3}{E_m^2k_m^2}\frac{L}{R}$	Negligible	Negligible
α_9	$-\frac{E_m^{-2}}{\exp(2\alpha_m t)}\iiint_V\langle-\tilde{\mathbf{u}}\cdot\nabla\tilde{p}\rangle\,\mathrm{d}V$	$-\frac{E_m^{-2}}{\exp(2\alpha_m t)}\iint_S\langle\mathbf{n}\cdot\tilde{\mathbf{u}}\,\tilde{p}\rangle\,\mathrm{d}S$	$\simeq \frac{9\pi^2M_b}{200E_m^2}\frac{L}{R}$
α_{10}	$\frac{E_m^{-2}}{\exp(2\alpha_m t)}\iiint_V\langle M_b(\hat{\mathbf{u}}+\tilde{\mathbf{u}})\cdot\nabla(\mathbf{U}\cdot\tilde{\mathbf{u}})\rangle\,\mathrm{d}V$	$-\frac{M_bE_m^{-2}}{\exp(2\alpha_m t)}\iint_S\langle\hat{\mathbf{n}}\cdot[\tilde{\mathbf{u}}(\mathbf{U}\cdot\tilde{\mathbf{u}})]\rangle\,\mathrm{d}S$	N/A[a]

[a]Flandro and Majdalani [3] ignore α_{10} due to uncertainties. However, Chibli et al. [2] and Fischbach et al. [15] show α_{10} opposite and equal to α_9.

$$\alpha_m = \alpha_1 + \alpha_2 + \alpha_3 + \alpha_6 + \alpha_7 \tag{4}$$

From Table 1 it is noted that only α_7 is connected to the mode number k_m in the form of the so-called penetration number ξ

$$\xi = \frac{k_m^2 \delta_{Re}^2}{M_b^3} \tag{5}$$

Chibli et al. [2] and Fischbach et al. [15] both note that a small ξ assumption has been made, that is $\xi < 1$. For the test motor used, the penetration number becomes larger than 1, after the fifth mode. Therefore, analysis will be limited to the first five modes observed experimentally.

C. Flandro's Energy Balance Method

Flandro [13,14] originally proposed that the growth can be described by one variable, ϵ, the normalized system amplitude. This analysis includes the classical linear stability computations and includes a nonlinear loss mechanism due to the formation of steep fronted waves forming. Subsequently [7–9] an additional design equation was included to predict the mean pressure shift. The design equations are two nonlinear coupled ordinary differential equations

$$\begin{cases} \frac{\mathrm{d}\varepsilon}{\mathrm{d}t} = \alpha^{(1)}\varepsilon + \alpha^{(2)}\varepsilon^2 + \cdots \\ \frac{\mathrm{d}\bar{p}}{\mathrm{d}t} = \beta_{\mathrm{DC}}^{(1)} + \beta_{\mathrm{DC}}^{(2)}\varepsilon^2 \end{cases} \tag{6}$$

$\alpha^{(1)}$ is the linear growth constant of the first mode. $\alpha^{(2)}$ is the first nonlinear term and is regarded here to be only shock wave losses. This analysis can be extended to higher orders but there are no known higher order interactions. To be able to apply these equations it is necessary to calculate the linear stability, shock wave losses and the mean pressure shift.

1. Shock Wave Losses

Flandro first included shock wave losses [13,14] and it has been used to good effect in prediction algorithms [6–9,16]. The only nonlinear contribution is that of a steep fronted shock wave [8,9]:

$$\iiint_V \left\langle \frac{\delta_{Re}^2}{(\gamma-1)Pr}\nabla^2 T + \delta_d^2(\nabla\cdot\mathbf{u})^2 \right\rangle \mathrm{d}Vy \tag{7}$$

This is the entropy gain and energy loss associated with steep fronted waves. Flandro et al. [8,9] notes this term has traditionally been ignored because it is only of significance when there is a very steep gradient in particle velocity and temperature. Acoustic waves rarely are of such high amplitudes that this becomes a significant factor, indeed the smaller the acoustic wave's amplitude the more negligible it becomes.

Treating the shock wave as an area of nonuniformity, Eq. (7) can be manipulated to yield the energy loss for a steep fronted wave [8,9]:

$$\left(\frac{\mathrm{d}E}{\mathrm{d}t}\right)_{\mathrm{shock}} = -\frac{S_{\mathrm{port}}}{\gamma(\gamma-1)}\frac{(s_2-s_1)*}{C_v} = \left(\frac{\varepsilon_{\mathrm{shock}}}{\bar{p}}\right)^3 S_{\mathrm{port}}\left(\frac{\gamma+1}{12\gamma^3}\right) \tag{8}$$

This leads to the following approximation:

$$\alpha^{(2)} = -\frac{(\gamma+1)}{3E^2}\left(\frac{\sigma}{2\gamma}\right)^3 S_{\mathrm{port}} \tag{9}$$

Where σ is dependent on the waveform that is assumed and S_{port} is the area of the shock front. For axial or longitudinal waves this is the cross-sectional area of the duct at a convenient location. For a cylindrical grain motor [6,13]

$$\alpha^{(2)} = \left(\frac{\gamma+1}{6\gamma}\right)\frac{a_0}{L} \tag{10}$$

2. Mean Pressure Shift

A dc pressure shift or mean pressure shift is often observed. It is closely linked to the growth of the limit amplitude of the acoustic wave. It is demonstrated that the mechanism that drives oscillations is the same as that for the dc pressure shift.

Ad hoc terms such as velocity coupling, burning surface velocity rectification, and acoustic erosivity that have been included in many analysis can be discarded. From the continuity equation the source of the dc pressure shift is readily obtained. By expanding and time averaging the equation the nonlinear terms are also retained [8,9]. The following is obtained [8]:

$$\frac{\mathrm{d}\bar{p}}{\mathrm{d}t} = -\nabla\cdot(M_b\bar{\rho}) - \frac{\varepsilon^2}{\gamma}\nabla\langle p'\mathbf{u}'\rangle \tag{11}$$

The first term here represents the quasi-steady mass flux from the surface and the mass leaving through the nozzle. Integrating over the volume of the chamber:

$$\frac{\mathrm{d}\bar{p}}{\mathrm{d}t} = \begin{Bmatrix} -\frac{1}{V}\iint_S \mathbf{n}\cdot(\rho\bar{M}_b\mathbf{U})\,\mathrm{d}S \\ -\varepsilon^2\left(\frac{1}{\gamma V}\right)\iint_S \mathbf{n}\cdot\langle p'\cdot\mathbf{u}'\rangle\,\mathrm{d}S \end{Bmatrix} \tag{12}$$

where

$$\mathbf{n}\cdot\langle p'\mathbf{u}'\rangle = \begin{cases} -\frac{1}{\gamma}M_b A_b^{(r)}\langle (p')^2\rangle & \text{(a) Waves Normal to Surface} \\ -\frac{M_b}{\gamma}(A_b^{(r)}+1)\langle (p')^2\rangle & \text{(b) Waves Parallel to Surface} \end{cases} \tag{13}$$

IV. Culick's Nonlinear Method

Culick [17,18] obtains second-order nonlinear equations for the mode amplitudes η_n

$$\ddot{\eta}_n + \omega_n^2\eta_n = 2\alpha_n\dot{\eta} + 2\theta_n\omega_n\eta_n - \overbrace{\sum_{i=1}^{\infty}\sum_{j=1}^{\infty}[A_{nij}\dot{\eta}_i\dot{\eta}_j + B_{nij}\eta_i\eta_j]}^{\text{Non-Linear Gas Dynamics}} \tag{14}$$

$2\alpha_n\dot{\eta}$ and $2\theta_n\omega_n\eta_n$ represent the linear interactions, the nonlinear gas dynamics is represented by the summation equation. For small fluctuations, $|\eta_n| \ll 1$, η_n can be represented as follows:

$$\eta_n(t) \approx r_n\cos(\omega_n t - \phi(t)) = A_n(t)\sin(\omega_n t) + B_n(t)\cos(\omega_n t) \tag{15}$$

Paparizos and Culick [19] presented truncated equations for $\mathrm{d}A_n/\mathrm{d}t$ and $\mathrm{d}B_n/\mathrm{d}t$ for longitudinal modes in a cylindrical motor

$$\frac{\mathrm{d}A_n}{\mathrm{d}t} = \alpha_n A_n + \theta_n B_n + \overbrace{\frac{n\beta_c}{2}\sum_{i=1}^{n-1}(A_i A_{n-i} - B_i B_{n-i})}^{\text{term1}} - \overbrace{n\beta_c\sum_{i=1}^{m-n}(A_{n+i}A_i - B_{n+i}B_i)}^{\text{term2}} \tag{16}$$

$$\frac{\mathrm{d}B_n}{\mathrm{d}t} = \alpha_n B_n - \theta_n A_n + \overbrace{\frac{n\beta_c}{2}\sum_{i=1}^{n-1}(A_i B_{n-i} + B_i A_{n-i})}^{\text{term3}} + \overbrace{n\beta_c\sum_{i=1}^{m-n}(A_{n+i}B_i - B_{n+i}A_i)}^{\text{term4}} \tag{17}$$

β_c represents the only term arising from the nonlinear gas dynamics

$$\beta_c = \frac{(1+\gamma)\omega_1}{8\gamma} \tag{18}$$

Culick's [10] cylindrical case α and θ values are used to evaluate these truncated results. Equations (16) and (17) are integrated forward in time.

V. Calculating the Admittance Function

A. Flandro's Method

From Eq. (6) it is possible to obtain an admittance function from the acoustic wave amplitude and the mean pressure shift. For a tubular grain assuming that shock wave losses are the only nonlinear mechanism, the change in acoustic wave amplitude for longitudinal modes becomes [6,13,14]

$$\frac{\mathrm{d}\epsilon}{\mathrm{d}t} = \epsilon\alpha_m - \epsilon^2\left(\frac{\gamma+1}{6\gamma}\right)\frac{\bar{a}}{L} \tag{19}$$

When the limit amplitude is reached $\mathrm{d}\epsilon/\mathrm{d}t = 0$. Thus, Eq. (19) can be rearranged to give

$$\alpha_m = \epsilon_{\text{limit}}\left(\frac{\gamma+1}{6\gamma}\right)\frac{\bar{a}}{L} \tag{20}$$

The admittance function is contained within α_1. Rearranging Eq. (3)

$$\alpha_1 = \alpha_m - \sum_{i=2}^{N}\alpha_i \tag{21}$$

Internal ballistic data is used to calculate the α values. The admittance function can now be calculated for each mode individually. An admittance function can also be obtained from the mean pressure shift. When the new mean pressure is reached $\mathrm{d}p/\mathrm{d}t = 0$. This means the pressure is no longer changing [8]

$$0 = \left[\beta_{\text{DC}}\frac{(p_0\bar{p})^{n-b}}{a_0}S_b - \bar{p}\left(\frac{2}{\gamma+1}\right)^{\frac{(\gamma+1)}{2(\gamma-1)}}S_{\text{throat}}\right] - \frac{\varepsilon^2}{\gamma}\iint_S \mathbf{n}\cdot\langle p'\cdot\mathbf{u}'\rangle\,\mathrm{d}S \tag{22}$$

Using the results from Eq. (13) and after some algebraic manipulation, the admittance can be calculated as follows [8]:

$$\frac{p_{\text{lim}}}{p_{\text{std}}} = \left[1 + \frac{\varepsilon^2 C_2}{4\gamma^2}(A_b^{(r)} + C_1)\right]^{\left(\frac{1}{1-n_b}\right)} \tag{23}$$

The n_b is the burning rate exponent, the pressure ratio is that of the measured mean pressure and the expected mean pressure if there was no instability, and C_1 is 0 when waves are normal and 1 when they are parallel

$$C_2 = \frac{1}{S_b}\iint_S \psi^2(\mathbf{r})\,\mathrm{d}S \tag{24}$$

C_2 accounts for the effective mode shape of a wave. For longitudinal waves it can be assumed to be approximately 0.5 [8]. It is now possible to solve for the admittance function. This method is limited to the first mode only. Flandro accounts for the losses due to nonlinear gas dynamics as a single shock front. This greatly simplifies the prediction of stability, however, it has limitations as an analysis tool.

B. Culick's Method

Culick's method allows for more than one mode to be evaluated. One of the major obstacles for this method has been computational expense. The amount of calculations required increase exponentially as the number of modes are increased. In the mid 1980s to early 1990s a large amount of work was done following on from Culick's analytical work [17,18] and Levine and Culick's numerical work [20,21]. Many analyses were reduced to only consider two modes to reduce computational effort. This is no longer an obstacle.

The results shown in Fig. 1 are calculated from the values for α and θ presented by Culick [10]. Identical results are obtained by French [6] for the same data set. Figures 1a–1c show the results when the published θ values are used, and Figs. 1d–1f show the results if θ for all modes are set equal to zero. Identical results are obtained as also shown by French [6]. Inspecting Eqs. (17) and (18) it is noted that the frequency shift essentially transfers energy from A_n to B_n and vice versa. Figures 1a–1c shows that A_n and B_n are 180° out of phase. Using random θ values do not alter the limit amplitude, it only alters the period of oscillation of A_n and B_n and thus the time it takes to reach the limit amplitude.

Recognizing that when A_n is at its maximum, B_n is equal to zero and also that when $\mathrm{d}A_n/\mathrm{d}t$ is equal to zero, $\mathrm{d}B_n/\mathrm{d}t$ is at a maximum, the converse is also true. When θ_n is set to zero, either A_n or B_n is at a

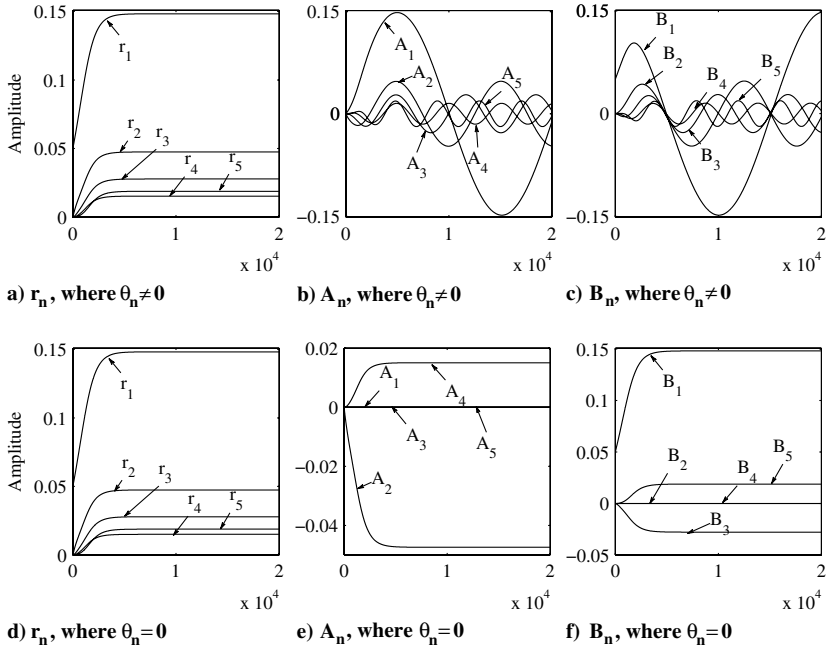

Fig. 1 Amplitude (p'/P) vs time steps (0.00001 s), produced from Culick's tubular grain data [6].

maximum, and correspondingly the matching amplitude is set to zero. Essentially it is being assumed that all modes are in phase with either A_n and B_n at a maximum or a minimum. It can be shown that for odd modes, $n = 1, 3, 5, \ldots$

$$B_n = r_n \sin\left(\frac{\pi}{2}n\right) \qquad A_n = 0 \tag{25}$$

For even modes, $n = 2, 4, 6, \ldots$

$$A_n = r_n \cos\left(\frac{\pi}{2}n\right) \qquad B_n = 0 \tag{26}$$

Furthermore, it is now possible to obtain α_n for each mode using Eqs. (16) and (17). For odd modes, $n = 1, 3, 5, \ldots$

$$\alpha_n = -\Bigg[-\theta_n A_n + \overbrace{\frac{n\beta_c}{2}\sum_{i=1}^{n-1}(A_i B_{n-i} + B_i A_{n-i})}^{\text{term3}} + \overbrace{n\beta_c \sum_{i=1}^{m-n}(A_{n+i}B_i - B_{n+i}A_i)}^{\text{term4}}\Bigg] \Big/ B_n \tag{27}$$

For even modes, $n = 2, 4, 6, \ldots$

$$\alpha_n = -\Bigg[\theta_n B_n + \overbrace{\frac{n\beta_c}{2}\sum_{i=1}^{n-1}(A_i A_{n-i} - B_i B_{n-i})}^{\text{term1}} - \overbrace{n\beta_c \sum_{i=1}^{m-n}(A_{n+i}A_i - B_{n+i}B_i)}^{\text{term2}}\Bigg] \Big/ A_n \tag{28}$$

The mode amplitudes, r_n published by French [6] are used. Exactly the same α values are obtained (cf. Table 2).

When using this method it is important to remember that Eqs. (16) and (17) are truncated. The last several modes' α values will be erroneous since their value is more strongly linked to the subsequent modes. When only 5 modes are used only α 1 and 2 are correct. As more modes are added the values of α_3 and α_4 change until their values are no longer affected by higher modes. Inspecting term 2 and term 4 of Eqs. (16) and (17) it can be seen that these terms are only interconnected to higher modes. An iterative process is used to evaluate for a specific mode if enough modes are taken into account to return a valid α.

VI. Cylindrical Motor Data Analysis

The tubular grain motor was pulsed tested with a HTPB/APC composite propellant. After firing a pulse, oscillations occurred and a mean pressure shift was observed (see Fig. 2). The signal was then divided into windows equal to the period of the first longitudinal mode. These windows were then evaluated using an FFT algorithm. This is a relatively simple method for calculating the amplitude growth of the individual modes.

Table 2 Mode stability α (s^{-1})

Mode	1	2	3	4	5
Published [6,10]	81.4	−316	−561	−874	−1256
Calculated	81.4	−316	−561	−874	−1255

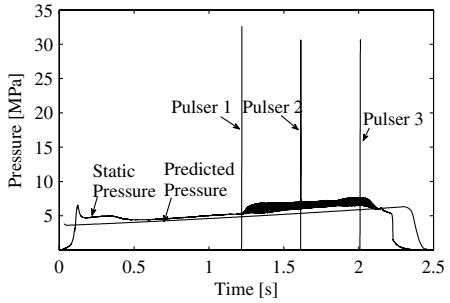

Fig. 2 First motor firing pressure profile prediction and experimental results.

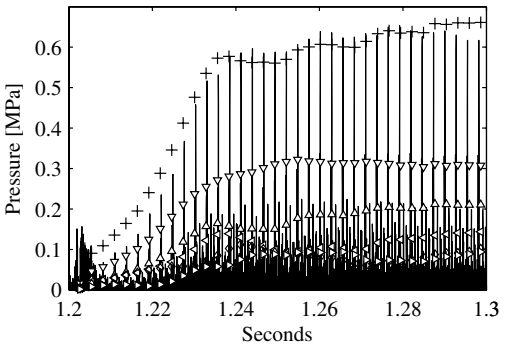

- Normalized wave + System Amplitude ▽ 1^{st} Mode △ 2^{nd} Mode ◁ 3^{rd} Mode ◇ 4^{th} Mode ▷ 5^{th} Mode

Fig. 3 Pulsed motor firing and individual modes.

In Fig. 3 it can be seen that after the initial plateau region is reached the amplitude remains constant for several cycles, and then the limiting amplitude readjusts to changing motor conditions. This is due to the dynamic behavior of the motor. Once instability occurs the limiting amplitude constantly readjusts to increasing burning area, increased volume, change in mean pressure, and changing mean flow velocity. The limit amplitude reached first will be used since this is the point closest to stable operating conditions. At this point the normalized system amplitude is 0.15. Furthermore, 25 modes were used to obtain the $\alpha_{1\text{–}10}$ on Table 3 using Culick's method.

Table 3 gives α_1 obtained from both methods and $\alpha_{2\text{–}10}$ from Culick's method. Flandro's method obtains $\alpha_1 = 35.6\ s^{-1}$, for a system amplitude of, $\epsilon \approx 0.15$. The linear analysis gives $A_b^{(r)} = 1.61$. α_1 obtained using Culick's method is 38.3 s^{-1} with $A_b^{(r)} = 1.67$. This shows relatively good agreement between the two methods. This result shows that using cylindrical motors to obtain an admittance function is indeed possible. If the test motor is modified so that ξ remains less than one for higher modes it should be possible to evaluate even more modes simultaneously. This can easily be achieved by increasing the length of the motor. Revaluating α_7 to include $\xi > 1$ should also be attempted.

Figure 4 shows the admittance curve calculated from the $\alpha_{1\text{–}5}$ obtained using Culick's method. This curve shows agreement with those of Blomshield et al. [22]. Blomshield et al. used a similar propellant with an HTPB binder and an array of stability additives for their T-Burner investigation. The trends observed are similar to the peak response being observed between 800–1200 Hz.

The admittance function obtained from the mean pressure shift is found to be, $A_b^{(r)} = 4.6$. This corresponds more closely with the admittance found for the third and fourth modes. There is clearly

Table 3 $\alpha_{1\text{–}10}$ (s^{-1}) at 5.3 MPa

Mode	1	2	3	4	5	6	7	8	9	10
Flandro	35.6	——	——	——	——	——	——	——	——	——
Culick	38.3	59.9	64.5	31.7	−32.4	−80.1	−103	−232	−240	−242

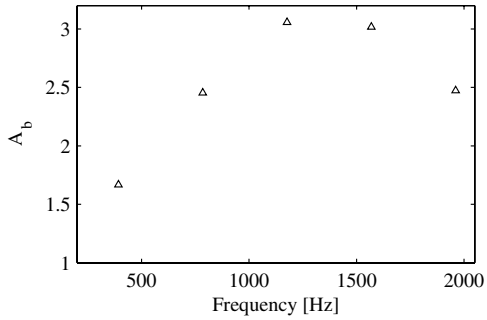

Fig. 4 Admittance curve obtained.

some refinement required to be able to use this method with confidence as mentioned by Flandro [8].

VII. Motors with Stability Additives

A. Stability Integrals

Particle dampening is an extremely useful tool as a suppressing agent for Combustion Instability. In modern tactical motors that are required to be smokeless ZrC particles have become the particles of choice. However, adding particles reduce the SRM performance (more inert particles mean less propellant).

The linear stability integrals do not need to be altered for this motor. The particle dampening can be added to Eq. (20). The most commonly used expression for particulate dampening will be used [22]

$$\alpha_p = \frac{C_m}{(1+C_m)}\frac{\omega}{2}\frac{\omega\tau_D}{1+(\omega\tau_D)^2} \tag{29}$$

The relaxation time τ_D is given as

$$\tau_D = \frac{\rho_p D^2}{18\mu} \tag{30}$$

B. Pulsed Test Results

1% SiC/LC replaced an equivalent mass of APC. Three motors with SIC additives were also pulsed 3 times. The first motor's pressure range was set to 4–6 MPa and was stable to the first two pulses only going unstable after the third pulse (cf. Fig. 5a). The second motor's operating pressure was set to 5–8 MPa and was also pulsed unstable after the first pulse (cf. Fig. 5b). Both these motor's pulsers were set to the maximum pulse level obtainable from the hardware. The final motor's operating pressure was also set to 5–8 MPa but the pulsers were set to 50% of the maximum. The motor only went unstable after the second pulse (cf. Fig. 5c). Two approaches were followed to evaluate all pulses that were damped out. Firstly, the classical linear analysis is employed

$$\epsilon(t) = e^{\alpha t} \tag{31}$$

The natural logarithm is taken of the normalized amplitude, a straight line is fitted to the data and the slope of this line is α. As with the unstable case the decaying wave's data is windowed and evaluated with the FFT algorithm. Fitting a straight line to this data gives an α for each mode. Figure 6 shows the nonlinear prediction using α_1 obtained from the linear analysis. The experimental results deviates from the predicted values due to the transducer noise being of the same order as the decaying wave. Using the linear analysis, on both the system amplitude and the amplitude of the first mode, the same value for α was obtained. This indicates that using the, FFT algorithm does give a correct result and that the α values obtained are representative of the modes stability.

The second method used was fitting Flandro's energy balance Eq. (19) to the system amplitude. This method is once again limited as it only gives the α for the first mode. The α values obtained using both methods showed excellent agreement (cf. Table 4).

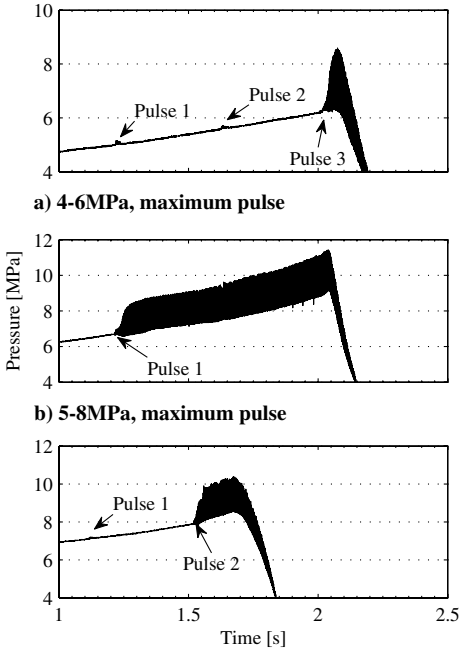

a) 4-6MPa, maximum pulse

b) 5-8MPa, maximum pulse

c) 5-8MPa, 50% maximum pulse

Fig. 5 Motors with stability additives pressure time history.

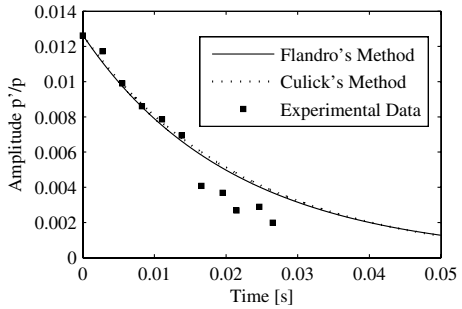

Fig. 6 Stability prediction from linear analysis.

The data analysis used when the motor is unstable is the same as for the motor with no stability additives. The limit amplitude is found using the FFT algorithm. Both Culick's and Flandro's methods were used. From the results in Table 4 it can be seen that the additives have increased the motor stability greatly. It can also be seen that the stability decreases with burn time. It is noted that investigations by Baum and Levine [23,24] and Blomshield et al. [25,26] have found that stability decreases towards the end of the burn time. This can be attributed to increased pressure in progressive burning grains (increased response), decrease in mean flow velocity and decreased nozzle dampening.

The addition of the particles has reduced the surface response dramatically and seemingly more than would be expected. It has been

Table 4 Example of linear and nonlinear data analysisα_{1-5} (s^{-1}) for motor 1

		Pulse 1 at 5.0 MPa			
Mode	1	2	3	4	5
Flandro	−46.4	——	——	——	——
Linear	−44.7	−50.7	−78.7	−84.2	−157
		Pulse 2 at 5.6 MPa			
Flandro	−39.1	——	——	——	——
Linear	−46.0	−41.0	−73.1	−84.7	−111
		Pulse 3 at 6.3 MPa			
Flandro	72.3	——	——	——	——
Culick	72.3	67.7	−8.14	−159	−382

documented that addition of particles can both reduce and increase the pressure-coupled response [22] with significant deviation from the baseline propellant. There may, however, be several contributing factors.

SiC is not commonly used and no information could be found that has been published on its use. It was chosen due to its good thermal properties, high melting temperature (2730°C), and availability. SiC in this reactive environment may form SiO_2. This, reaction if it takes place at the propellant surface, may have a significant affect on the response of the propellant. At the motor operating temperature SiO_2 is a liquid; this can result in particle amalgamation altering the particle size distribution causing the particle dampening predictions to be incorrect.

A second factor may be increased surface losses. The addition of the new particles changes the propellant surface properties. This can have a significant affect on the ability of the burning process to drive the acoustic waves. Several tests will still be performed with SiC as an additive; this should give a clearer indication of the dominant dampening mechanism. SiC has shown itself to be a viable alternative as a stability additive.

The A_b values obtained when the motor is unstable is an order of magnitude larger than that when the motor is stable and corresponds more closely with that of the baseline propellant (cf. Fig. 7). The increase in admittance as the pressure increases is coupled to a corresponding increase in burn rate. Looking back at some of the very first investigations by Denison and Baum [27] a pressure fluctuation has several local effects. These effects cause a moving burning zone that in some way provides energy to the acoustic wave. At higher pressures even small disturbances can have a more noticeable effect. As the amplitude grows the local effects become even more pronounced. The admittance is not only a propellant property at a specific pressure but also the acoustic pressure of a disturbance. It should be expected that at the same mean pressure the admittance function obtained from a pulse where the motor remains stable should be different to that of a motor that is unstable. Counter balancing the ever increasing response of the propellant is the nonlinear increase due to the steepening of the wave resulting in a limiting amplitude.

This is often referred to as triggering, or more correctly the system has received enough broadband energy to excite a steep fronted wave. There is always low level instability present [8,9] however the amplitude increases so slowly it is indistinguishable from the transducer noise in most cases. The limitation of T-Burners is that the admittance function obtained is that of the propellant when unstable. This value allows for an accurate prediction of the limit amplitude but not necessarily at what pulse amplitude the motor will be excited into forming a steep fronted wave. Careful design of a test matrix should allow for triggering to be studied more closely and the admittance function can be evaluated in terms of not only the mean pressure but also the magnitude of the acoustic pressure. To be able to take full advantage of this capability will require careful evaluation of the relationship between the acoustic pressure, mean pressure and the admittance function. Figure 7 shows all these trends. The first two

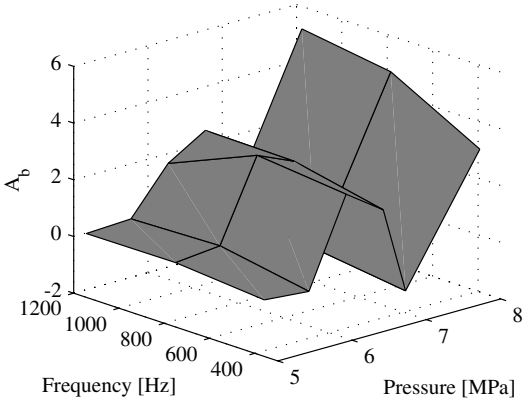

Fig. 7 Admittance obtained for motor with additives.

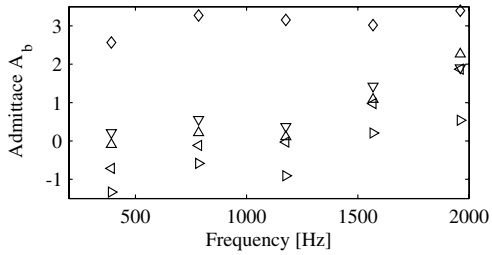

▷ at 4.3MPa, ◁ at 4.7MPa, △ at 5.2 MPa, ▽ at 6.5MPa, ◇ at 7MPa

Fig. 8 Al admittance curves.

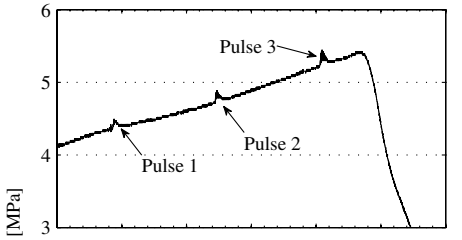

a) 3.5-5.5MPa, maximum pulse

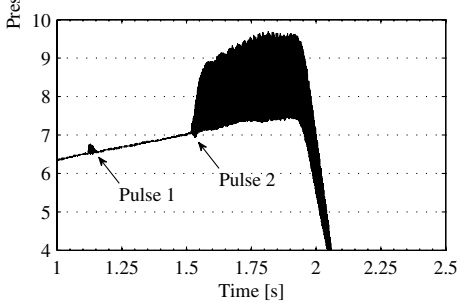

b) 5-8MPa, maximum pulse

Fig. 9 Motors with 4% Al pressure time history.

sets of data at 5.1 and 5.7 MPa are from the first test and are the stable pulses. The admittance increases as the pressure increases and the disturbance is approximately the same. The second two sets and final set of admittance curves obtained at 6.2, 6.7, and 8 MPa show the admittance obtained when the motor is unstable. The admittance curve obtained at 7 MPa reveals the importance of the pulse amplitude. Though at a higher mean pressure the admittance value is quite low in comparison with other tests, however, the pulse amplitude magnitude was 50% of the previous tests resulting in a muted propellant response. As the pressure increases the transport properties and density change correspondingly; this has an effect on the penetration number. ξ increases such that only the first three modes can be used with confidence after the third pulse. The surface plot (Fig. 7) therefore only uses the first three modes' admittance values. Two motors with 4% Al have also been tested. These motors proved significantly more stable than the SiC counterparts, due to the increase in particle loading and different particle size ranges. The first motor with an expected operating range from 3.5–5.5 MPa was pulsed 3 times at maximum pulse strength and remained stable (see Fig. 9). The second Al motor had an operating range between 5–8 MPa and went unstable after the second pulse. As with the 1% SiC formulation the admittance function obtained again increased with the pressure increase for the same level pulse amplitudes (cf. Fig. 8). The admittance function obtained at 7 MPa is the admittance once the motor has gone unstable. This again shows the importance of triggering. The results for the unstable admittance correlate well with the admittance curve of a similar Al propellant published by Blomshield et al. [22].

VIII. Conclusions

It has been demonstrated that a pulsed tubular grain motor can be used to obtain an admittance function. Three different composite propellants were tested and results obtained for all three correspond well with published literature. Linear theory for such a configuration is well established with analytical results. The two predominant nonlinear theories have both given comparable results. It has been shown that both can be used as analysis tools. Culick's method, however, allows for multiple modes to be evaluated.

Triggering can be evaluated. This is arguably the most vital information to a motor designer as this will allow for the prediction of the pulsed stability limit, i.e., what magnitude pulse will cause instability. Furthermore this information can be compared with the maximum pulse that a motor could feasibly experience during operation.

Ideally a test would consist of three pulses with only the last pulse causing instability. This will allow three different pressures to be evaluated with a minimum of five modes yielding reliable results. This will mean that a minimum of 15 data points will be collected that otherwise would have required 15 T-Burner tests.

This method is still in the initial phases of development and several issues need to be addressed such as reevaluation of α_7 for $\xi > 1$. This will enable the evaluation of more modes simultaneously. An alternative solution would be to increase the aspect ratio of the motor by increasing the length of the motor. These obstacles can be overcome yielding ever improving results from such tests.

The data is windowed to the length of period of the first fundamental longitudinal mode. When evaluating higher modes using the FFT algorithm it is important to realize that several cycles will have been completed and thus the amplitude at this point is an average value during this time period.

References

[1] Rousseau, C. W., Knoetze, J. H., and Steyn, S. F., "Establishing a Cost Effective and Innovative Combustion Instability Programme," *44th AIAA/ASME/SAE/ASEE Joint Propulsion Conference & Exhibit*, AIAA Paper No. 2008-4603, Hartford, CT, 2008.

[2] Chibli, H. A., Majdalani, J., and Flandro, G. A., "Fundamental Growth Rate Corrections in Rocket Motor Stability Calculations," *38TH AIAA/ASME/SAE/ASEE Joint Propulsion Conference and Exhibit*, AIAA Paper No. AIAA-2002-3610, Indianapolis, IN, 2002.

[3] Flandro, G. A., and Majdalani, J., "Aeroacoustic Instability in Rockets," *AIAA Journal*, Vol. 41, No. 3, 2003, pp. 485–497. doi:10.2514/2.1971

[4] Fischbach, S. R., Flandro, G. A., and Majdalani, J., "Volume-to-Surface Transformations of Rocket Stability Integrals," *40th AIAA/ASME/SAE/ASEE Joint Propulsion Conference and Exhibit*, AIAA Paper No. AIAA-2004-4053, Fort Lauderdale, FL, 2004.

[5] Fischbach, S. R., Majdalani, J., and Flandro, G. A., "Acoustic Instability of the Slab Rocket Motor," *Journal of Propulsion and Power*, Vol. 23, No. 1, 2007, pp. 146–157. doi:10.2514/1.14794

[6] French, J. C., "Non-Linear Combustion Instability Predicition of SRMS using SPP/SSP," *39th AIAA/ASME/SAE/ASEE Joint Propulsion Conference*, AIAA Paper No. 2003-4668, 2003.

[7] Flandro, G. A., Perry, E. H., and French, J. C., "Nonlinear Rocket Motor Stability Computations: Understanding the Brownlee-Marble Observations," *44th AIAA Aerospace Sciences Meeting and Exhibit*, AIAA Paper No. AIAA-2006-539, Reno, NV, 2006, pp. 6538–6558.

[8] Flandro, G. A., Majdalani, J., and French, J. C., "Incorperation of Nonlinear Capabilities in the Stability Prediction Program," *40th AIAA/ASME/SAE/ASEE Joint Propulsion Conference and Exhibit*, AIAA Paper No. AIAA-2004-4182, Fort Lauderdale, FL, 2004.

[9] Flandro, G. A., Fischbach, S. R., and Majdalani, J., "Nonlinear Rocket Stability Prediction: Limit Amplitude, Triggering, and Mean Pressure Shift," *40th AIAA/ASME/SAE/ASEE Joint Propulsion Conference and Exhibit*, AIAA Paper No. AIAA-2004-4054, Fort Lauderdale, FL, 2004.

[10] Culick, F. E. C., "Some Recent Advances for Nonlinear Acoustics in Combustion Chambers," *AIAA Journal*, Vol. 32, No. 1, 1994, pp. 146–169. doi:10.2514/3.11962

[11] Culick, F. E. C., "Non-Linear Growth and Limiting Amplitude of Acoustic Oscillations in Combustion Chambers," *Combustion Science and Technology*, Vol. 3, No. 1, 1971, pp. 1–16. doi:10.1080/00102207108952266

[12] Culick, F. E. C., "Combustion Instabilities: Mating Dance of Chemical, Combustion, and Combustor Dynamics," *36th AIAA/ASM/SAE/ASEE Joint Propulsion Conference and Exhibit*, AIAA, Reston, VA, 2000.

[13] Flandro, G. A., "Approximate Analysis of Nonlinear Instability with Shock Waves," *18th AIAA/SAE/ASME Joint Propulsion Conference*, AIAA Paper No. AIAA-82-1220, New York, 1982.

[14] Flandro, G. A., "Energy Balance Analysis of Nonlinear Combustion Instability with Shock Waves," *Journal of Propulsion and Power*, Vol. 1, No. 3, 1985, pp. 210–221. doi:10.2514/3.22783

[15] Fischbach, S., Majdalani, J., Flandro, G., and French, J., "Verification and Validation of Rocket Stability Integral Transformations," *41st AIAA/ASE/SAE/ASEE Joint Propulsion Conference and Exhibit*, AIAA Paper No. 2005-4001, 2005.

[16] Flandro, G. A., Malhortha, S., and Gazra, D. M., "Nonlinear Combustion Instability Data Reduction," *AIAA/ASME/SAE/ASEE Joint Propulsion Conference*, AIAA Paper No. AIAA-96-3251, Lake Buena Vista, FL, 1996.

[17] Culick, F. E. C., "Nonlinear Behaviour of Acoustic Waves in Combustion Chambers-I," *Acta Astronautica*, Vol. 3, Nos. 9–10, 1976, pp. 715–734. doi:10.1016/0094-5765(76)90107-7

[18] Culick, F. E. C., "Nonlinear Behaviour of Acoustic Waves in Combustion Chambers-II," *Acta Astronautica*, Vol. 3, Nos. 9–101976, pp. 735–757. doi:10.1016/0094-5765(76)90108-9

[19] Paprizos, L. G., and Culick, F. E. C., "The Two-Mode Approximation to Non-linear Acoustics in Combustion Chambers," *Combustion Science and Technology*, Vol. 65, No. 1, 1989, pp. 39–65. doi:10.1080/00102208908924041

[20] Levine, J. N., and Culick, F. E. C., "Numerical Analysis of Longitudinal Combustion Instability in Metallized Solid Rocket Motors," Ultrasystems, Inc. Tech. Rept. AFRPL-TR-72-88, 1972.

[21] Levine, J. N., and Culick, F. E. C., "Nonlinear Analysis of Solid Rocket Combustion Chambers," Air Force Rocket Propulsion Labratory Tech. Rept. AFRPLTR-74-45, 1974.

[22] Blomshield, F. S., Stalnake, R. A., and Beckstead, M. W., "Combustion Instability Additive Investigation," AIAA Paper No. 1999-2226, 1999.

[23] Baum, J. D., Levine, J. N., and Lovine, R. L., "Pulsed Instability in Rocket Motors: A Comparison Between Predictions and Experiments," *Journal of Propulsion and Power*, Vol. 4, No. 4, 1988, pp. 308–316. doi:10.2514/3.23068

[24] Baum, J. D., and Levine, J. N., "Modeling of Nonlinear Longitudinal Instability in Solid Rocket Motors," *Acta Astronautica*, Vol. 13, Nos. 6–7, 1986, pp. 339–348. doi:10.1016/0094-5765(86)90089-5

[25] Blomshield, F. S., Mathes, H. B., Crump, J. A., and Bieter, C. A., "Nonlinear Stability Testing of Full-Scale Tactical Motors," *Journal of Propulsion and Power*, Vol. 13, No. 3, 1997, pp. 356–366. doi:10.2514/2.5192

[26] Blomshield, F. S., Crump, J. A., Mathes, H. B., and Beckstead, M. W., "Stability Testing of Full Scale Tactical Motors," *Journal of Propulsion and Power*, Vol. 13, No. 3, 1997, pp. 349–355. doi:10.2514/2.5191

[27] Denison, M. R., and Baum, E., "A Simplified Model of Unstable Burning in Solid Propellants," *ARS Journal*, Vol. 31, No. 8, Aug. 1961, pp. 1112–1122.

S. Son
Associate Editor